On the Low Risk of SSR in Type III Wind Turbines Operating in Grid-Forming Control

Preprint

Weihang Yan, Shahil Shah, Vahan Gevorgian, Przemyslaw Koralewicz, and Robb Wallen

National Renewable Energy Laboratory

Presented at the 21st Wind & Solar Integration Workshop
The Hague, Netherlands
October 12–14, 2022

NREL is a national laboratory of the U.S. Department of Energy
Office of Energy Efficiency & Renewable Energy
Operated by the Alliance for Sustainable Energy, LLC

This report is available at no cost from the National Renewable Energy Laboratory (NREL) at www.nrel.gov/publications.

Contract No. DE-AC36-08GO28308

Conference Paper
NREL/CP-5D00-83808
July 2023

On the Low Risk of SSR in Type III Wind Turbines Operating in Grid-Forming Control

Preprint

Weihang Yan, Shahil Shah, Vahan Gevorgian, Przemyslaw Koralewicz, and Robb Wallen

1 National Renewable Energy Laboratory

Suggested Citation
Yan, Weihang, Shahil Shah, Vahan Gevorgian, Przemyslaw Koralewicz, and Robb Wallen. 2023. *On the Low Risk of SSR in Type III Wind Turbines Operating in Grid-Forming Control: Preprint*. Golden, CO: National Renewable Energy Laboratory. NREL/CP-5D00-83808. https://www.nrel.gov/docs/fy23osti/83808.pdf.

NREL is a national laboratory of the U.S. Department of Energy
Office of Energy Efficiency & Renewable Energy
Operated by the Alliance for Sustainable Energy, LLC

This report is available at no cost from the National Renewable Energy Laboratory (NREL) at www.nrel.gov/publications.

Contract No. DE-AC36-08GO28308

Conference Paper
NREL/CP-5D00-83808
July 2023

National Renewable Energy Laboratory
15013 Denver West Parkway
Golden, CO 80401
303-275-3000 • www.nrel.gov

NOTICE

This work was authored by the National Renewable Energy Laboratory, operated by Alliance for Sustainable Energy, LLC, for the U.S. Department of Energy (DOE) under Contract No. DE-AC36-08GO28308. Funding provided by U.S. Department of Energy Office of Energy Efficiency and Renewable Energy Wind Energy Technologies Office. The views expressed herein do not necessarily represent the views of the DOE or the U.S. Government. The U.S. Government retains and the publisher, by accepting the article for publication, acknowledges that the U.S. Government retains a nonexclusive, paid-up, irrevocable, worldwide license to publish or reproduce the published form of this work, or allow others to do so, for U.S. Government purposes.

This report is available at no cost from the National Renewable Energy Laboratory (NREL) at www.nrel.gov/publications.

U.S. Department of Energy (DOE) reports produced after 1991 and a growing number of pre-1991 documents are available free via www.OSTI.gov.

Cover Photos by Dennis Schroeder: (clockwise, left to right) NREL 51934, NREL 45897, NREL 42160, NREL 45891, NREL 48097, NREL 46526.

NREL prints on paper that contains recycled content.

On the Low Risk of SSR in Type III Wind Turbines Operating in Grid-Forming Control

Weihang Yan, Shahil Shah, Vahan Gevorgian, Przemyslaw Koralewicz, Robb Wallen
National Renewable Energy Laboratory (NREL)
Golden, CO. 80401, USA
{Weihang.Yan; Shahil.Shah; Vahan.Gevorgian; Przemyslaw.Koralewicz; Robb.Wallen}@nrel.gov

***Abstract*—We have shown in previous work that the risk of subsynchronous resonance between wind power plant with Type III wind turbines and a series-compensated transmission line is low when the wind turbines are operated in grid-forming mode, instead of the standard grid-following mode. This paper explains the fundamental mechanism behind the improved damping characteristics by modeling the positive- and negative-sequence impedances of Type III wind turbines in grid-forming control mode. It is discovered that the grid-forming control naturally acts against the negative resistance behavior of Type III wind turbines at subsynchronous frequencies that results from an interaction between the rotor-side converter current controller and negative slip. The developed sequence impedance models and improved damping behavior are verified using PSCAD simulations of a 2.5-MW Type III grid-forming wind turbine. The modeling predictions are also supported by experimentally measuring the sequence impedance response of a 2.5-MW Type III wind turbine in grid-forming control mode.**

***Index Terms*—Subsynchronous resonance, impedance modeling, grid-forming control, grid-following control, stability.**

I. Introduction

The root cause of subsynchronous resonance (SSR) in standard Type III wind turbines is well researched. Existing commissioned Type III wind turbines operate in grid-following (GFL) mode, in which they are controlled as current sources feeding the electric grid. The impedance modeling of standard Type III GFL wind turbines has demonstrated that they exhibit negative resistance, and hence negative damping at subsynchronous frequencies. Moreover, it is also shown that the negative resistance is due to the proportional gain of the current controller in the turbine's rotor-side converter (RSC) getting divided by the frequency-dependent slip; the latter is negative at subsynchronous frequencies and consequently creates negative resistance in the wind turbine impedance [1]–[3]. The negative resistance can reduce the damping of potential resonance between the wind turbine generator, which presents inductive characteristics, and the series compensation capacitors inserted in transmission lines. Hence, manufacturers are required to reduce the risk of SSR events in Type III wind turbines through appropriate design, such as adding additional damping controllers and modifying the filter design [1].

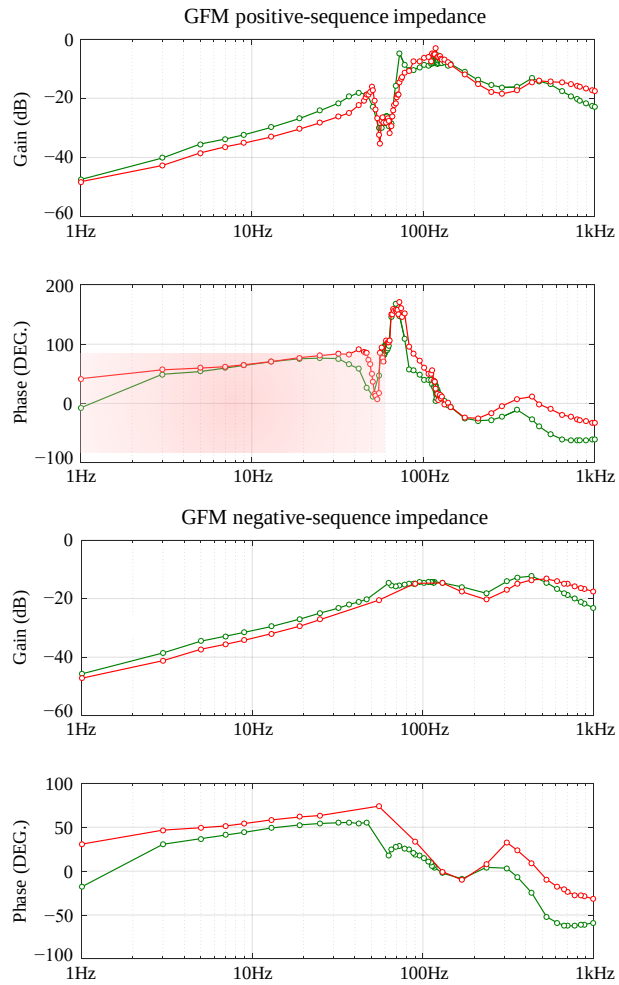

Fig. 1: Experimental impedance measurements of the 2.5-MW Type III wind turbine in GFM control. Red: turbine operation at 1460 rpm with 2-MW power output. Green: turbine operation at 1100 rpm with 0.9-MW power output. Circles: sampling points.

The control and operation of inverter-based resources (IBR) in grid-forming (GFM) mode has captivated the attention of power system engineers. GFM resources become one of potential solutions to maintain the stability of power systems with

This work was authored by the National Renewable Energy Laboratory, operated by Alliance for Sustainable Energy, LLC, for the U.S. Department of Energy (DOE) under Contract No. DE-AC36-08GO28308. Funding provided by U.S. Department of Energy Office of Energy Efficiency and Renewable Energy Wind Energy Technologies Office. The views expressed in the article do not necessarily represent the views of the DOE or the U.S. Government. The U.S. Government retains and the publisher, by accepting the article for publication, acknowledges that the U.S. Government retains a nonexclusive, paid-up, irrevocable, worldwide license to publish or reproduce the published form of this work, or allow others to do so, for U.S. Government purposes.

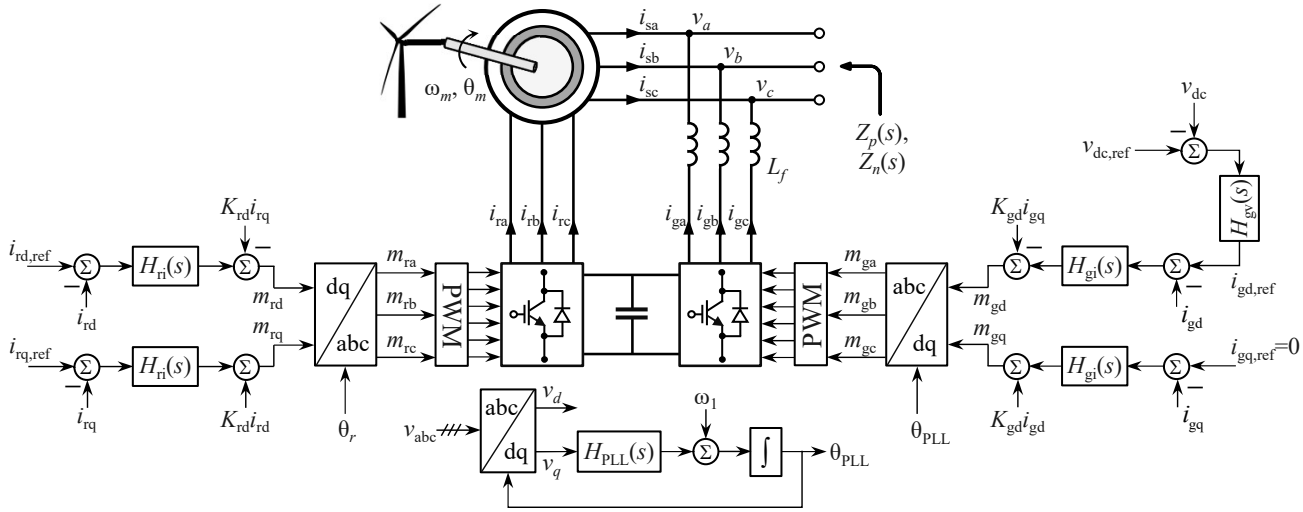

Fig. 2: Control and circuit diagram of a Type III wind turbine

high levels of IBRs in which they are controlled as voltage sources, similar to synchronous generators [4]. Recent studies confirmed the positive role of GFM inverters in improving system stability, such as [5] demonstrated that GFM inverters are less likely to experience harmonic resonance in a weak grid. As a result, significant efforts are now directed toward operating PV inverters and wind turbines in GFM control [4]–[7].

We have demonstrated Type III GFM wind turbines, unlike GFL turbines, exhibit positive resistance at subsynchronous frequencies, reducing the risk of SSR when wind turbines are within close proximity of series-compensated transmission lines [8]. This was surprising because the current control design of doubly-fed induction generator (DFIG) is not changed, which has been confirmed to be responsible for the negative resistance in Type III GFL wind turbines [2]. We are also currently testing a 2.5-MW Type III wind turbine in GFM control at the Flatirons Campus of the National Renewable Energy Laboratory (NREL) in Colorado, United States [9]. Impedance measurements conducted on the Type III wind turbine in GFM control using the 7-MW controllable grid interface (CGI) also revealed its positive resistance behavior. Although the impedance measurement captured the stability characteristics of the Type III GFM wind turbine looking from the turbine's point of common coupling, it is important to understand whether the improved damping is dependent on certain control parameter design or whether there is a fundamental mechanism that improves the damping characteristics such that SSR is less likely in Type III wind turbines when they are operated in GFM control.

This paper presents the impedance measurements done on the 2.5-MW Type III wind turbine when it is operated in GFM control. To pinpoint the positive resistance behavior in GFM turbines at subsynchronous frequencies, the positive- and negative-sequence impedance models of Type III wind turbines in GFM control are developed and validated. The developed impedance models explain the fundamental mechanism of how the GFM control mitigates the classic negative resistance behavior associated with Type III wind turbines. The developed sequence impedance models show that the positive damping at subsynchronous frequencies is a fundamental characteristic of Type III GFM wind turbines and not an outcome of a specific parameter design; hence, GFM control can potentially eliminate the SSR problem in Type III wind turbines, which has plagued many wind power plants around the world.

II. Experimental Impedance Measurements

This section presents the impedance measurements of the Type III GFM wind turbine using the impedance measurement system at the Flatirons Campus of NREL [10]. The hardware test setup includes a 2.5-MW GFM wind turbine driven by a 5-MW dynamometer. The wind turbine under test [9] is connected to the 7-MW/13.2-kV CGI, via a 3-MVA, 690-V/13.2-kV step-up transformer. Fig. 1 shows the impedance measurements of the GFM wind turbine. The impedance measurements experimentally confirmed the positive resistance behavior of the Type III GFM wind turbines, where the impedance phase response is confined within −90 degrees to +90 degrees at subsynchronous frequencies (highlighted in the red box in Fig. 1). Furthermore, such positive damping behavior at subsynchronous frequencies from the GFM turbine is not dependent on a specific operating condition. To understand the fundamental mechanism that improves the damping characteristics in Type III wind turbines when they are operated in GFM control, sequence impedance models are developed in the following section using the GFM control design in [8] for Type III wind turbines.

III. Sequence Impedance Modeling

A. Grid-Forming Control of Type III Wind Turbines

Fig. 2 and Fig. 3 describe the GFM turbine control diagrams adopted in this paper. The letters "s" and "r" indicate variables correlate to the stator and rotor windings of the DFIG, respectively, and the letter "g" indicates variables correlate to

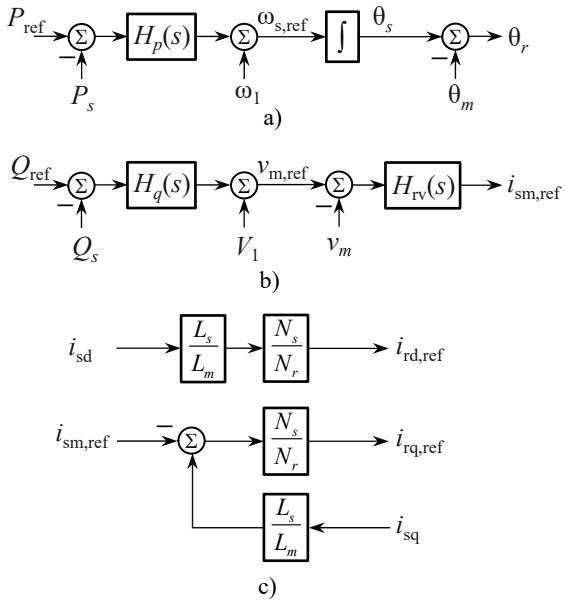

Fig. 3: GFM outer-loop control for Type III wind turbines. (a). active power to frequency control; (b). reactive power to voltage control; and (c). reference for the d-q components of the rotor currents.

the grid-side converter (GSC). K_{rd} and K_{gd} are the current controller decoupling gains.

The control and operation of Type III wind turbines in GFM control, different from GFL control, internally sets the frequency $\omega_{\text{s,ref}}$ and magnitude $v_{\text{m,ref}}$ of the DFIG stator voltage through active power to frequency controller $H_p(s)$, and reactive power to voltage controller $H_q(s)$. The voltage controller, $H_{\text{rv}}(s)$, generates the reference of the magnetizing current, $i_{\text{sm,ref}}$, for the DFIG depending on the feedback of the stator voltage magnitude v_m. The rotating reference frame used for RSC current control is aligned with the stator voltages according to (1) and (2). More details can be found in [8].

$$i_{\text{rd,ref}} = \frac{N_s}{N_r}\frac{L_s}{L_m} i_{\text{sd}} \tag{1}$$

$$i_{\text{rq,ref}} = -\frac{N_s}{N_r} i_{\text{sm,ref}} + \frac{N_s}{N_r}\frac{L_s}{L_m} i_{\text{sq}} \tag{2}$$

Here, $L_s = L_{\text{ls}} + L_m$ is the stator self-inductance.

Note that the RSC inner-loop current control for Type III GFM wind turbines is identical to that of GFL wind turbines. Further, the controls of the GSC remain the same for both GFM and GFL control modes of wind turbines. The detailed circuit parameters of a Type III wind turbine are listed in Table. I, and the designed control parameters and system steady states are in Table. II.

B. Sequence Impedance Modeling

Under a positive-sequence, small-signal voltage perturbation at frequency $\omega_p = 2\pi f_p$, the phase a terminal voltage of a Type III wind turbine in time domain is:

$$v_a(t) = \sqrt{\frac{2}{3}} V_1 \cos(\omega_1 t) + V_p \cos(\omega_p t + \phi_{vp}) \tag{3}$$

TABLE I: Circuit Parameters in PSCAD Simulation

Parameter	Value
DFIG rated power	2.5 MW
Nominal frequency, f_1	60 Hz
DFIG rated voltage, V_1	690 V
Converter DC voltage, v_{dc}	2000 V
Modulation gain, k_m	0.5
Rotor Speed, ω_m	1.3 p.u.
Stator to rotor turns ratio, N_s/N_r	0.379
Stator resistance, R_s	0.0054 p.u.
Reflected rotor resistance, $R_r{}'$	0.00607 p.u.
Stator leakage inductance, L_{ls}	0.102 p.u.
Reflected rotor leakage inductance, $L_{\text{lr}}{}'$	0.110 p.u.
Magnetizing inductance, L_m	4.362 p.u.
GSC filter inductance, L_f	0.3 mH
DC bus capacitor, C_{dc}	20 mF

TABLE II: Converter Control Parameters

Power smoothing filter, $G_P(s) = 1/(0.02s+1)$	
RSC current controller, $H_{\text{ri}}(s) = 0.000456 + 0.0505/s$	
GSC current controller, $H_{\text{gi}}(s) = 0.000269 + 0.338/s$	
GSC DC voltage controller, $H_{\text{gv}}(s) = 4.206 + 529.1/s$	
Steady state stator winding current, $\mathbf{I}_{s0} = 3011.96 - j1072.76$ A	
Steady state rotor winding current, $\mathbf{I}_{r0} = 1165.09 - j650.06$ A	
Steady state GSC current, $\mathbf{I}_{g0} = 994.2 + j0$ A	
Steady state RSC modulation signals, $\mathbf{M}_{r0} = -0.52 - j0.10$	
Steady state GSC modulation signals, $\mathbf{M}_{g0} = 0.56 - j0.11$	
GFM	GFL
Active power compensator:	Power compensator:
$H_p(s) = 3 + 0.2/s$	$H_p(s) = 0 + 0.0108/s$
Reactive power compensator:	PLL compensator
$H_q(s) = 0.2 + 1/s$	$H_{\text{PLL}}(s) = 0.237 + 44.6/s$
Voltage compensator:	
$H_{\text{rv}}(s) = 1.2 + 6.67/s$	

where V_p and ϕ_{vp} correspond to the magnitude and phase of the positive-sequence perturbation at frequency f_p. Turbine voltage under perturbation can be transformed in frequency domain as:

$$\mathbf{V}_a[f] = \begin{cases} \frac{1}{2}V_1 & f = f_1 \\ \mathbf{V}_p & f = \pm f_p \end{cases} \tag{4}$$

where $\mathbf{V}_p = (V_p/2)e^{\pm j\phi_{\text{vp}}}$. Voltages of phase b and phase c follow the same notation. Three phase currents can be similarly described in complex form. In this paper, bold letters are used to represent the complex form of variables after Fourier transform. Then, the positive-sequence impedance of a Type III wind turbine, $Z_p(s)$, is defined as the ratio of $V_p(s)$ to $-[I_{\text{sp}}(s) + I_{\text{gp}}(s)]$, where $I_{\text{sp}}(s)$ and $I_{\text{gp}}(s)$ are the perturbations of output currents from DFIG stator and GSC, respectively [5], [10]. The dynamics of the DFIG stator current, $I_{\text{sp}}(s)$, is described as:

$$\left[s(L_{\text{ls}} + L_{\text{lr}}{}') + R_s + \frac{R_r{}'}{\sigma_p(s)}\right] \cdot I_{\text{sp}}(s) = \frac{k_m V_{\text{dc}}}{\sigma_p(s)}\frac{N_s}{N_r} M_{\text{rp}}(s - j\omega_m) - V_p(s) \tag{5}$$

where the frequency-dependent gain $\sigma_p(s)$ in (6) maps the frequency shift between the stator and rotor sides due to the machine slip [3]:

$$\sigma_p(s) = \frac{s - j\omega_m}{s} \tag{6}$$

Because of the voltage perturbation, the synchronous frame is displaced from the rotating frame of the grid voltage by angle of $\Delta\theta(t)$. Assuming the initial phase of the stator voltage as $\theta_0(t) = \omega_1 t$, the phase of the DFIG stator voltage, $\theta_s(t)$, can be written as:

$$\theta_s(t) = \theta_0(t) + \Delta\theta(t) \tag{7}$$

Then, implementing Park's transformation, the stator voltages of the DFIG in the frequency domain are derived as:

$$\mathbf{V}_d[f] = \begin{cases} V_1 & f = 0 \\ \mathbf{V}_p & f = \pm(f_p - f_1) \end{cases} \tag{8}$$

$$\mathbf{V}_q[f] = \begin{cases} 0 & f = 0 \\ \mp j\mathbf{V}_p - V_1\Delta\boldsymbol{\theta}[f] & f = \pm(f_p - f_1) \end{cases} \tag{9}$$

The currents in the DFIG's rotor winding, $\mathbf{I}_{\mathrm{rd}}$ and $\mathbf{I}_{\mathrm{rq}}$, can be presented as:

$$\mathbf{I}_{\mathrm{rd}}[f] = \begin{cases} I_{\mathrm{rd0}} & f = 0 \\ \mathbf{I}_{\mathrm{rp}} + I_{\mathrm{rq0}}\Delta\boldsymbol{\theta}[f] & f = \pm(f_p - f_1) \end{cases} \tag{10}$$

$$\mathbf{I}_{\mathrm{rq}}[f] = \begin{cases} I_{\mathrm{rq0}} & f = 0 \\ \mp j\mathbf{I}_{\mathrm{rp}} - I_{\mathrm{rd0}}\Delta\boldsymbol{\theta}[f] & f = \pm(f_p - f_1) \end{cases} \tag{11}$$

The currents in the DFIG's stator winding, $\mathbf{I}_{\mathrm{sd}}$ and $\mathbf{I}_{\mathrm{sq}}$, can be similarly derived. The rotor winding currents can be reflected in the DFIG's stator winding by applying:

$$I_{\mathrm{rp}}(s - j\omega_m) = \frac{N_s}{N_r} I_{\mathrm{sp}}(s) \tag{12}$$

Instantaneous power of DFIG are linearized as in (13) and (14) with steady-state v_q equals to 0:

$$P_s(s) = \frac{3}{2} G_p(s)[I_{\mathrm{sd0}} V_d(s) + I_{\mathrm{sq0}} V_q(s) + V_1 I_{\mathrm{sd}}(s)] \tag{13}$$

$$Q_s(s) = \frac{3}{2} G_p(s)[-I_{\mathrm{sq0}} V_d(s) + I_{\mathrm{sd0}} V_q(s) - V_1 I_{\mathrm{sq}}(s)] \tag{14}$$

Then, the modulating signals of the RSC respecting the *d-q* reference frame can be derived as in (15) and (16), based on RSC inner loop current control:

$$M_{\mathrm{rd}}(s) = -H_{\mathrm{ri}}(s) I_{\mathrm{rd}}(s) - K_{\mathrm{rd}} I_{\mathrm{rq}}(s) + H_{\mathrm{ri}}(s) I_{\mathrm{rd,ref}}(s) \tag{15}$$

$$M_{\mathrm{rq}}(s) = -H_{\mathrm{ri}}(s) I_{\mathrm{rq}}(s) + K_{\mathrm{rd}} I_{\mathrm{rd}}(s) + H_{\mathrm{ri}}(s) I_{\mathrm{rq,ref}}(s) \tag{16}$$

Assuming the DC-link capacitor is sufficiently large, the DC bus voltage, v_{dc}, can be considered constant for the simplicity of impedance modeling.

Based on (1) and (2), the dynamics of RSC current references are converted as in (17) and (18), combining the reactive power to voltage controller:

$$I_{\mathrm{rd,ref}}(s) = \frac{N_s}{N_r}\frac{L_s}{L_m} I_{\mathrm{sd}}(s) \tag{17}$$

$$\begin{aligned} I_{\mathrm{rq,ref}}(s) = {} & \frac{N_s}{N_r}\frac{L_s}{L_m} I_{\mathrm{sq}}(s) + \\ & \frac{N_s}{N_r} H_{\mathrm{rv}}(s)[H_q(s) Q_s(s) + V_m(s)] \end{aligned} \tag{18}$$

where, the linearized voltage magnitude $V_m(s)$ of the DFIG stator voltage is derived as:

$$V_m(s) = V_d(s) \tag{19}$$

where steady-state v_d and v_q equal to V_1 and 0, respectively.

Combining the linearized reactive power, equations (14) and (17)–(19) complete the modeling of the voltage control loop of Type III GFM wind turbines. Furthermore, the dynamics of the phase angle of the DFIG stator voltage are derived from active power to frequency controller, as in:

$$\Delta\theta(s) = -\frac{1}{s} H_p(s) P_s(s) \tag{20}$$

Then, the linearized active power (13) is taken into (20) to complete the frequency control loop of the GFM wind turbines. Substituting (8)–(20) into (5), the detailed positive-sequence impedance model of the DFIG is derived as in (21) when the Type III wind turbine is controlled in GFM mode. $T_p(s) = G_p(s)H_p(s)/s$ represents the active power loop gain, and $T_q(s) = G_p(s)H_q(s)H_{\mathrm{rv}}(s)H_{\mathrm{ri}}(s)$ represents the reactive power loop gain. Combining the impedance of GSC, the positive-sequence impedance of the Type III wind turbine, $Z_p(s)$, is then described as:

$$Z_p(s) = \frac{Z_{\mathrm{sp}}(s) \cdot Z_{\mathrm{gp}}(s)}{Z_{\mathrm{sp}}(s) + Z_{\mathrm{gp}}(s)} \tag{22}$$

where the positive-sequence impedance of the GSC [3] is given as:

$$Z_{\mathrm{gp}}(s) = \frac{sL_f + k_m V_{\mathrm{dc}}[H_{\mathrm{gi}}(s - j\omega_1) - jK_{\mathrm{gd}}]}{1 - \frac{1}{2} k_m V_{\mathrm{dc}}\{I_{g0}[H_{\mathrm{gi}}(s - j\omega_1) - jK_{\mathrm{gd}}] + M_{g0}\}\frac{T_{\mathrm{PLL}}(s - j\omega_1)}{V_1}} \tag{23}$$

$T_{\mathrm{PLL}}(s) = V_1 H_{\mathrm{PLL}}(s)/[1 + V_1 T_{\mathrm{PLL}}(s)]$ denotes the closed-loop gain of the PLL (phase-locked loop). Here, it completes the full positive-sequence impedance model of Type III GFM wind turbines.

The positive-sequence impedance model of the DFIG is derived as in (24) when the Type III wind turbine is operating in GFL control mode. PI compensators, $H_p(s)$, are implemented on top of RSC current control as outer loop to regulate the power outputs of DFIG.

The impedance models derived so far are positive sequence. Negative-sequence impedances, $Z_n(s)$, can be derived using (25), for the Type III wind turbine in both GFL and GFM controls [10].

$$Z_n(s) = Z_p(-s)^* \tag{25}$$

Note that the cross-frequency coupling of a Type III wind turbine is weak at frequencies away from the fundamental frequency and, herein, ignored in this paper for the SSR stability analysis.

IV. Model Reduction and SSR Stability Analysis

To validate the developed sequence impedance models, a 2.5-MW/0.69-kV Type III wind turbine is developed in PSCAD, where the turbine control can be selected between GFM and GFL modes. Fig. 4 validates the developed sequence impedance models of the wind turbine in GFL and GFM controls. The phase response of the positive-sequence impedance for the GFL wind turbine crosses +90° at subsynchronous frequencies. This confirms the negative resistance behavior

Type III wind turbines in GFM control:

$$Z_{\mathrm{sp}}(s) = \frac{\begin{array}{l} R_s + \frac{R_r{}'}{\sigma_p(s)} + s\left(L_{\mathrm{ls}} + L_{\mathrm{lr}}'\right) + \frac{k_m V_{\mathrm{dc}}}{\sigma_p(s)}\left(\frac{N_s}{N_r}\right)^2 \left[\left(1 - \frac{L_s}{L_m}\right) H_{\mathrm{ri}}(s - j\omega_1) - jK_{\mathrm{rd}}\right] \\ +j\frac{3}{4}\frac{k_m V_{\mathrm{dc}}}{\sigma_p(s)}\frac{N_s}{N_r} V_1 \left[\left(\mathbf{I}_{r0} - \frac{N_s}{N_r}\frac{L_s}{L_m}\mathbf{I}_{s0}\right) H_{\mathrm{ri}}(s - j\omega_1) - j\mathbf{I}_{r0}K_{\mathrm{rd}} + \mathbf{M}_{r0}\right] T_p(s - j\omega_1) + \frac{3}{4}\frac{k_m V_{\mathrm{dc}}}{\sigma_p(s)}\left(\frac{N_s}{N_r}\right)^2 V_1 T_q(s - j\omega_1) \end{array}}{\begin{array}{l} 1 - j\frac{1}{2}\frac{k_m V_{\mathrm{dc}}}{\sigma_p(s)}\left(\frac{N_s}{N_r}\right)^2 H_{\mathrm{rv}}(s - j\omega_1) H_{\mathrm{ri}}(s - j\omega_1) \\ +j\frac{3}{4}\frac{k_m V_{\mathrm{dc}}}{\sigma_p(s)}\frac{N_s}{N_r}\mathbf{I}_{s0}{}^* \left[\left(\mathbf{I}_{r0} - \frac{N_s}{N_r}\frac{L_s}{L_m}\mathbf{I}_{s0}\right) H_{\mathrm{ri}}(s - j\omega_1) - j\mathbf{I}_{r0}K_{\mathrm{rd}} + \mathbf{M}_{r0}\right] T_p(s - j\omega_1) - \frac{3}{4}\frac{k_m V_{\mathrm{dc}}}{\sigma_p(s)}\left(\frac{N_s}{N_r}\right)^2 \mathbf{I}_{s0}{}^* T_q(s - j\omega_1) \end{array}} \tag{21}$$

Type III wind turbines in GFL control:

$$Z_{\mathrm{sp}}(s) = \frac{R_s + \frac{R_r{}'}{\sigma_p(s)} + s(L_{\mathrm{ls}} + L_{\mathrm{lr}}') + \frac{k_m V_{\mathrm{dc}}}{\sigma_p(s)}\frac{N_s}{N_r}\left\{\frac{N_s}{N_r}\left[H_{\mathrm{ri}}(s - j\omega_1) - jK_{\mathrm{rd}}\right] + \frac{3}{2}V_1 G_p(s - j\omega_1) H_p(s - j\omega_1) H_{\mathrm{ri}}(s - j\omega_1)\right\}}{1 - \frac{1}{2}\frac{k_m V_{\mathrm{dc}}}{\sigma_p(s)}\frac{N_s}{N_r}\left\{\mathbf{I}_{r0}\left[H_{\mathrm{ri}}(s - j\omega_1) - jK_{\mathrm{rd}}\right] + \mathbf{M}_{r0}\right\}\frac{T_{\mathrm{PLL}}(s - j\omega_1)}{V_1}} \tag{24}$$

that potentially leads to SSR instability. The developed model for GFM wind turbines has similar impedance characteristics to experimental measurements that does not exhibit negative resistance at subsynchronous frequencies, which lower the risk of SSR problems.

A. Impedance model reduction

Due to model complexity, sequence impedance models in (21) and (24) provide little information to pinpoint the mechanism of SSR for GFM and GFL wind turbines at subsynchronous frequencies. Hence, model reduction is further carried out in this section.

The GSC processes only a small portion of the total power; hence, ignoring $Z_{\mathrm{gp}}(s)$ does not significantly modify the impedance response of Type III wind turbines at subsynchronous frequencies. Further, PLL and turbine power control have little impact on the impedance response of GFL wind turbines that away from the fundamental frequency. Hence, the positive-sequence impedance model of Type III GFL wind turbines after the model reduction is:

$$\begin{aligned} Z_{p,\mathrm{GFL}}(s) \approx R_s + \frac{R_r{}'}{\sigma_p(s)} + \frac{k_m V_{\mathrm{dc}}}{\sigma_p(s)}\left(\frac{N_s}{N_r}\right)^2 k_{\mathrm{pr}} + \\ s\left(L_{\mathrm{ls}} + L_{\mathrm{lr}}'\right) + \frac{k_m V_{\mathrm{dc}}}{\sigma_p(s)}\left(\frac{N_s}{N_r}\right)^2 \left[\frac{k_{\mathrm{ir}}}{(s - j\omega_1)} - jK_{\mathrm{rd}}\right] \end{aligned} \tag{26}$$

where the PI compensator of the RSC current control is $H_{\mathrm{ri}}(s) = k_{\mathrm{pr}} + k_{\mathrm{ir}}/s$. The model in (26) can be equivalent to a series RLC circuit [2], in which the rotor winding resistance and the proportional gain of the RSC current controller collaboratively interact with the negative frequency dependent gain $\sigma_p(s)$ and contribute to the negative resistance at subsynchronous frequencies, causing higher risk of SSR instability.

The model reduction procedure for GFM wind turbines can be similarly performed by ignoring the outer-loop controls (power controller and voltage controller) because they are designed to be significantly slower in control bandwidths, such that they only impact the impedance response around the fundamental frequency. Therefore, the sequence impedance model of GFM wind turbines after the model reduction is,

$$\begin{aligned} Z_{p,\mathrm{GFM}}(s) \approx R_s + \frac{R_r{}'}{\sigma_p(s)} + \frac{k_m V_{\mathrm{dc}}}{-\sigma_p(s)}\left(\frac{N_s}{N_r}\right)^2 \frac{L_{\mathrm{ls}}}{L_m} k_{\mathrm{pr}} + \\ s\left(L_{\mathrm{ls}} + L_{\mathrm{lr}}'\right) + \frac{k_m V_{\mathrm{dc}}}{-\sigma_p(s)}\left(\frac{N_s}{N_r}\right)^2 \left[\frac{L_{\mathrm{ls}}}{L_m}\frac{k_{\mathrm{ir}}}{(s - j\omega_1)} + jK_{\mathrm{rd}}\right] \end{aligned} \tag{27}$$

By aligning RSC current vectors to the stator voltages' orientation in turbine GFM mode, the term associated with the proportional gain of the RSC current compensator is compensated (marked as red), and, further, adds a positive resistance to the turbine equivalent circuit. In fact, such compensation can be positive or negative, opposite to the sign of the frequency dependent gain. It behaves as a positive resistance with the negative frequency dependent gain at subsynchronous frequencies, lowering the risk of SSR. On the other hand, it behaves as a negative resistance at higher frequencies but its amplitude diminishes as the frequency-dependent gain increases.

The sequence impedance models in (27) also show that Type III GFM wind turbines can be equivalent to a RLC circuit without losing model accuracy at subsynchronous frequencies. Such circuit dynamics are verified from both the developed impedance models and the experimental impedance measurement. Fig. 4 confirms the validity of the performed impedance model reduction.

B. Impedance-based stability analysis

The simulated wind turbine is connected to a 33-kV, 50-MVA grid with the short-circuit ratio equal to 4 and X/R ratio equal to 10. The grid impedance, $Z_l(s)$, is marked as black in Fig. 4 with 50% series line compensation. The analytical predictions between the detailed and simplified models show almost identical conclusion in analyzing the turbine SSR stability. The developed impedance models predict an unstable SSR at 9 Hz, with a negative phase margin of $-76°$ ($= 180° - 256°$) for standard GFL wind turbines. The impedance models of GFM wind turbines, on the other hand, predict a

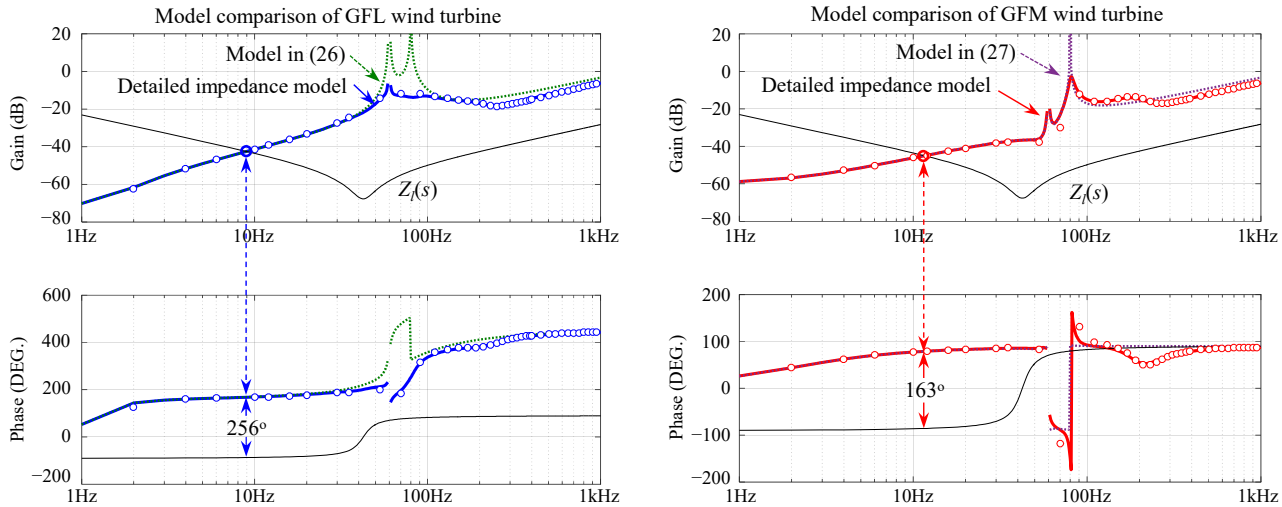

Fig. 4: Analytical model comparison and impedance-based stability prediction for Type III wind turbines in GFL and GFM control modes. Blue: detailed impedance model of a GFL turbine. Green, impedance model of a GFL turbine after the model reduction. Red: detailed impedance model of a GFM turbine. Purple: impedance model of a GFM turbine after the model reduction. Black: grid impedance. Dots: point-by-point PSCAD simulations

stable turbine operation at subsynchronous frequencies, with a phase margin of 17° (= 180°–163°). Time domain simulation in Fig. 5 verifies such analytical prediction. Reference [3] explained the inaccurate prediction for resonance frequency, limited by the small-signal modeling of grid impedance.

V. Conclusion

This paper presented the sequence impedance modeling of Type III wind turbines in GFM control mode. Model reduction is carried out, which equivalents GFM wind turbines to RLC circuits and pinpoints their stability characteristics. Both numerical simulations and experimental measurements support the validity of the developed impedance models.

The fundamental mechanism behind the improved SSR damping for Type III GFM wind turbines is explained through the developed impedance models. It is identified that the turbine GFM control, locking the rotor current vectors to DFIG stator voltages' orientation to be specific, naturally compensates the classic negative resistance behavior in Type III wind turbines, regardless of the turbine operating condition. Such stability property of Type III GFM wind turbines provides an potential solution to system operators for SSR damping without the need of designing additional damping controller. It further demonstrates the necessity of GFM resources in power system with high level of IBRs.

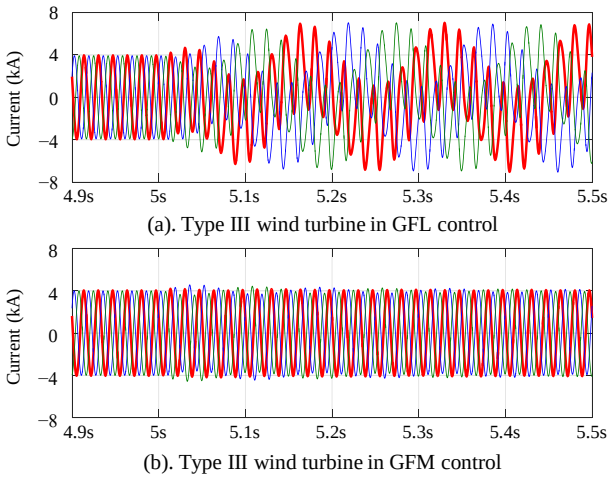

Fig. 5: Output currents of Type III wind turbine during SSR event: a) wind turbine in GFL control, b) wind turbine in GFM control.

References

[1] IEEE PES WindSSO Taskforce, "PES TR-80: Wind energy systems sub-synchronous oscillations: events and modeling, 2020," https://resourcecenter.ieee-pes.org/publications/technical-reports/PES-TP_TR80_AMPS_WSSO_070920.html.

[2] L. Fan and Z. Miao, "Nyquist-stability-criterion-based SSR explanation for type-3 wind generators," *IEEE Trans. on Energy Conv.*, vol. 32, no. 3, pp. 807–809, Sep. 2012.

[3] S. Shah, V. Gevorgian, and H. Liu, "Impedance-based prediction of SSR-generated harmonics in doubly-fed induction generators," *In Proc. IEEE Power & Energy Soc. Gen. Meeting*, 2019, pp. 1–5.

[4] ESIG High Share of Inverter-Based Generation TaskForce, "Grid-forming technology in energy systems integration, 2022," https://www.esig.energy/wp-content/uploads/2022/03/ESIG-GFM-report-2022.pdf.

[5] W. Yan, S. Shah, V. Gevorgian, and D. W. Gao, "Sequence impedance modeling of grid-forming inverters," *In Proc. IEEE Power & Energy Soc. Gen. Meeting*, 2021, pp. 1–5.

[6] W. Yan, L. Chen, S. Yan, and et al, "Enabling and evaluation of inertial control for PMSG-WTG using synchronverter with multiple virtual rotating masses in microgrid," *IEEE Trans. on Sustain. Energy*, vol. 11, no. 2, pp. 1078–1088, Apr. 2020.

[7] V. Gevorgian, S. Shah, W. Yan, and G. Henderson, "Grid-forming wind: getting ready for prime time, with or without inverters," *IEEE Electrifi. Mag.*, vol. 10, no. 1, pp. 52–64, Mar. 2022.

[8] S. Shah and V. Gevorgian, "Control, operation, and stability characteristics of grid-forming type III wind turbines," presented at the *Wind Integration Workshop*, Nov. 11-12, 2020.

[9] V. Gevorgian, S. Shah, W. Yan , and et al, "Grid forming wind power," presented at the *ESIG Spring Techn. Workshop*, Tucson, AZ, Mar. 21–24, 2022.

[10] S. Shah, P. Koralewicz, V. Gevorgian, and R. Wallen, "Sequence impedance measurement of utility-scale wind turbines and inverters – reference frame, frequency coupling, and MIMO/SISO forms," *IEEE Trans. on Energy Conv.*, vol. 37, no. 1, pp. 75–86, Mar. 2022.